
# The Magnetic Error Tolerances in SESAME Storage Ring Magnets

---

SES-TE-AP-TN-0004

July 8, 2014

Authored by: Maher Attal, Erhard Huttel

Reviewed by: Erhard Huttel

Approved by: Erhard Huttel

Access List : ---Internal ☐--------- External☐

SESAME, P.O. Box 7, Allan, 19252, Jordan, www.sesame.org.jo

REVISION HISTORY

| Revision | Date | Description | Author |
|---|---|---|---|
| | | | |

# Contents

*Abstract*

This note investigates the tolerance on magnetic errors in the SESAME storage ring which preserves reasonable optics, beam lifetime and injection efficiency. The magnetic errors compose errors in the main magnet field and the high order multipoles.

## 1. Introduction

The lattice of the 8-fold SESAME storage ring is a Double Bend Achromat with dispersion distribution in straight sections as seen in Fig. 1. The adopted lattice is a simple one with one family of bending magnets, two families of quadrupoles, and two families of sextupoles.

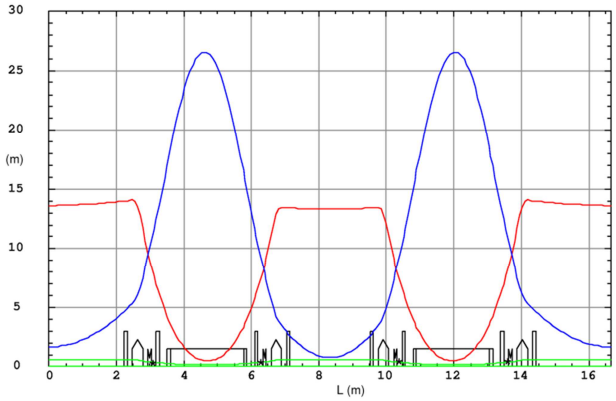


Figure 1: SESAME storage ring optics, with horizontal beta function $\beta_x$ (red), vertical beta function $\beta_z$ (blue), and dispersion $\eta_x$ (green).

For efficient injection into the storage ring and large electron beam lifetime a reasonable large dynamic aperture is required. Since the magnetic errors are a main source of dynamic aperture destruction, they should be investigated and their tolerance limits should be defined prior to the magnet construction. This report investigates the magnetic error tolerances of SESAME storage ring magnets: bending magnets, quadrupoles, and sextupoles. The magnetic errors compose:

- Magnetic flux and gradient errors due to variation in magnetic length and in magnetic gap in the same family magnets.
- Magnetic error due to the undesired systematic and random high order multipoles.

All the calculations are carried out for chromaticity corrected to +5 in both planes. Although we may not need to go to horizontal chromaticity +5 in the machine, nevertheless this value is used as a safety margin for the dynamic aperture. The corresponding sextupoles integrated strengths are $kl_{SF}$ = 1.05647 $m^{-2}$ and $kl_{SD}$ = -1.66657 $m^{-2}$ for focusing and defocusing sextupole respectively as given by BETA code. The different calculations in this report are done using the tracking codes BETA [1], Accelerator Toolbox [2], and TRACY-2 [3].

The impact of the investigated magnetic errors is mainly orbit distortion, tune shift with amplitude, and consequently dynamic aperture destruction. Hence, the tolerable magnetic errors should maintain a dynamic aperture that doesn't shrink to strongly smaller than the physical aperture and a reasonable orbit distortion which costs reasonable corrector strength to be corrected.

The dynamic aperture calculations are carried out at the middle of the long section which has a physical acceptance (x = ± 35 mm, y = ±3.5 mm) defined by the storage ring vacuum chamber with

dimensions (x = ± 35 mm, y = ±14 mm) scaled to the optical functions. The name "*chamber-limited dynamic aperture*" will be given to the dynamic aperture when the vacuum chamber limitation is included in the tracking calculations.

## 2. The error in magnetic length of bending magnets

The magnetic length error *Δ(Bl)/Bl* in the bending magnets distorts the horizontal orbit and consequently the dynamic aperture ( due to optical distortion in sextupoles) as shown in Fig.2 where 1 rms ΔB/B = 1 x$10^{-3}$ error is used. The closed orbit is tracked for 100 samples while the chamber-limited dynamic aperture is tracked for 50 samples.

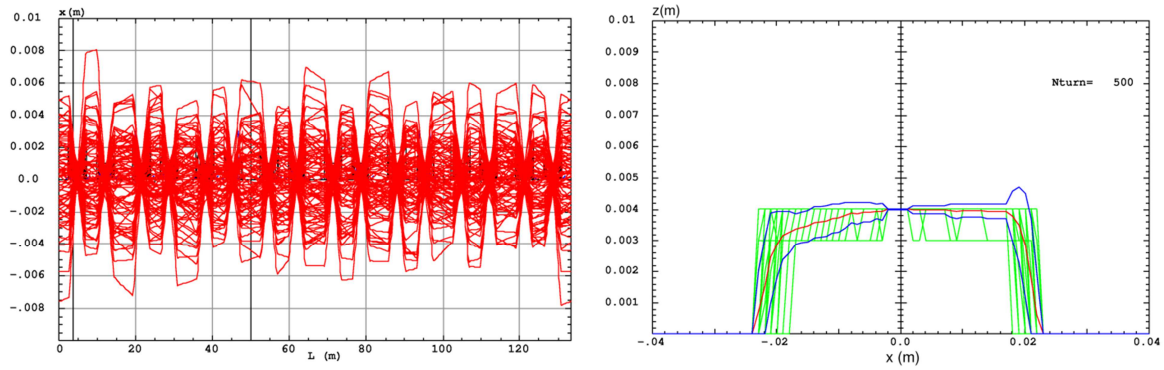


Figure 2: The potential distortions on the horizontal closed orbit (left), and on the chamber-limited dynamic aperture (right) due to 1 rms magnetic flux error ΔB/B = 1 x$10^{-3}$ in bending magnets. The red and blue dynamic apertures represent the average and the rms ones of 50 samples.

However to be more realistic, the magnetic length error should be considered taking into account also the other known sources of orbit distortion like the magnet misalignments. Figure 3 shows the distorted and corrected orbits using different values of ΔB/B: 1 x$10^{-3}$, 2 x$10^{-3}$, 3 x$10^{-3}$, and 5 x$10^{-3}$ taking into account also the magnet misalignment errors listed in Table 1.

| Misalignment | **Dipole** | **Quadrupole** | **Sextupole** |
|---|---|---|---|
| dx = ds, dz (mm) | 0.2, 0.1 | 0.1 | 0.1 |
| $d\phi_x = d\phi_y = d\phi_s$ (mrad) | 0.2 | 0.1 | 0.1 |

Table 1: Misalignment (shifts and rotations) tolerances for the storage ring magnets.

The closed orbit in SESAME is corrected using 64 BPMs and 32 correctors in each plane. The strength of horizontal correctors needed to correct each of the above orbit distortions are **0.08 mrad** for ΔB/B = 0, **0.16 mrad** for ΔB/B = 1 x$10^{-3}$, **0.28 mrad** for ΔB/B = 2 x$10^{-3}$, **0.34 mrad** for ΔB/B = 3 x$10^{-3}$, and **0.65 mrad** for ΔB/B = 5 x$10^{-3}$. It should be pointed out that the maximum strength of our correctors is 0.5 mrad.

Based on Fig. 3, and taking into a successful 1$^{st}$ injection into storage ring which allows for 5 mm as a maximum orbit distortion scheme at the 23 mm-displaced septum, one can say that **the dipole magnetic length *Δ(Bl)/Bl* should be *< 2 x$10^{-3}$ rms. The error distribution should be cutoff at 2σ.***

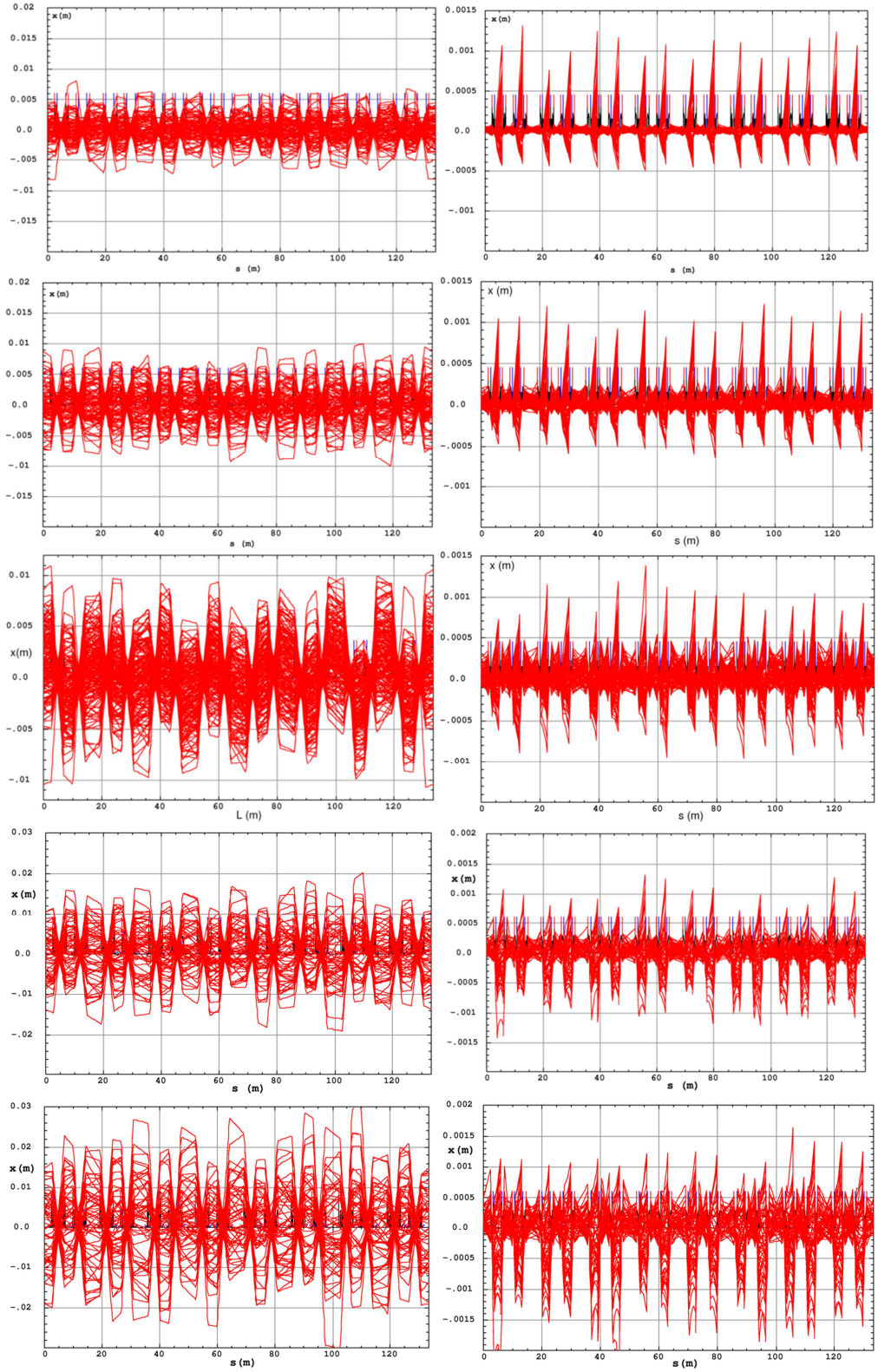


Figure 3: 100 samples of potential closed orbit before and after correction due to Table 1 errors with: bending magnet flux error $\Delta B/B = 0$ ((1,1), (1,2)), $\Delta B/B = 1 \times 10^{-3}$ ((2,1), (2,2)), $\Delta B/B = 2 \times 10^{-3}$ ((3,1), (3,2)), $\Delta B/B = 3 \times 10^{-3}$ ((4,1), (4,2)), $\Delta B/B = 5 \times 10^{-3}$ ((5,1), (5,2)).

### 3. The error in gap of the bending magnets

The variation in dipole gaps Δgap/gap should not result in integrated flux error more than the tolerance value 2 x$10^{-3}$. Hence ***Δgap/gap < 2 x$10^{-3}$ with error distribution cutoff at 2σ.***

### 4. The error in integrated gradient *Δ(Gl)/Gl* in bending magnets, quadrupoles, and sextupoles

The gradient error in the combined-function bending magnets and quadrupoles causes tune shifts, beta beating and dispersion beating which result, mainly, in destructing the dynamic aperture reducing in turn the injection efficiency and beam lifetime. The error in sextupole gradient doesn't affect the optics, to first order, however it distorts the chromaticity and nonlinear optical optimization which result at the end in destructing the on-momentum and off-momentum dynamic apertures. Figure 4 displays the different optical effects of 1 rms of ***Δ(Gl)/Gl = 3 x$10^{-3}$*** in bending magnets, quadrupoles and sextupoles using 25 samples. The dynamic apertures are tracked for 2000 turns with x = z = 0.5mm steps.

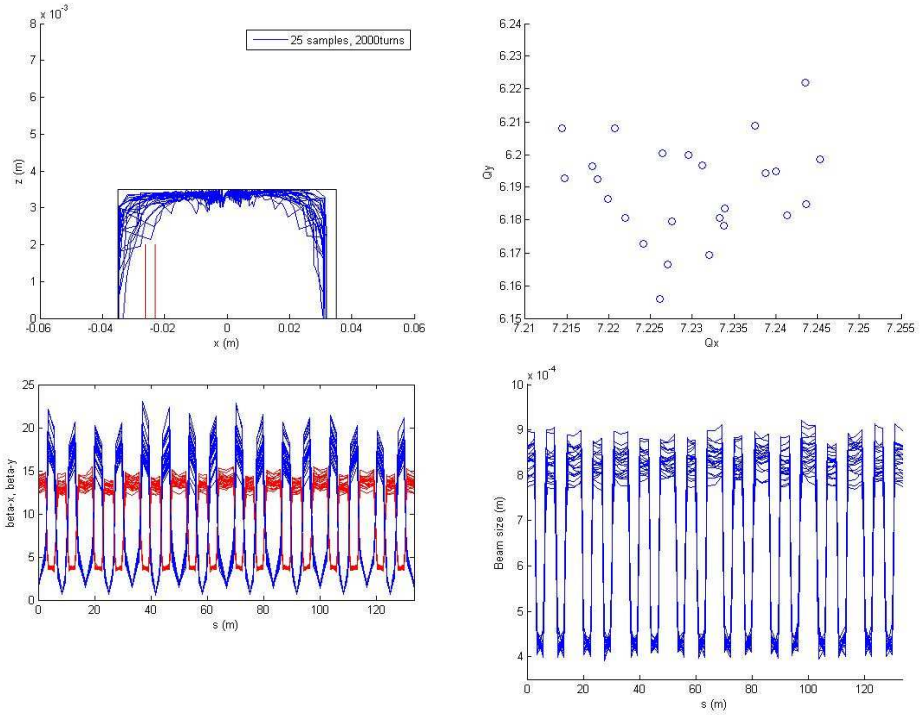


Figure 4: 25 samples of the optical distortions: (top-left) chamber-limited dynamic aperture, (top-right) tunes shift, (bottom-left) beta beating, and (bottom-right) vertical beam size, due to 1 rms value of the gradient error ΔG/G = 3 x $10^{-3}$ in all the bending, quadrupole, and sextupole magnets. In figure (top-left) the vacuum chamber physical acceptance is plotted in black and the injection septum sheet is in red.

It can be seen from Fig. 4 that the particle stability (represented by the dynamic aperture) is not so sensitive to the gradient errors in the lattice. This is due to the not so strong optical focusing.
The optics is less sensitive to gradient error in the defocusing quadrupole QD than that in the bending magnet or the focusing quadrupole. This is shown in Fig. 5 on the tune shift for example. Hence the tolerance on gradient error in QD can be more relaxed.

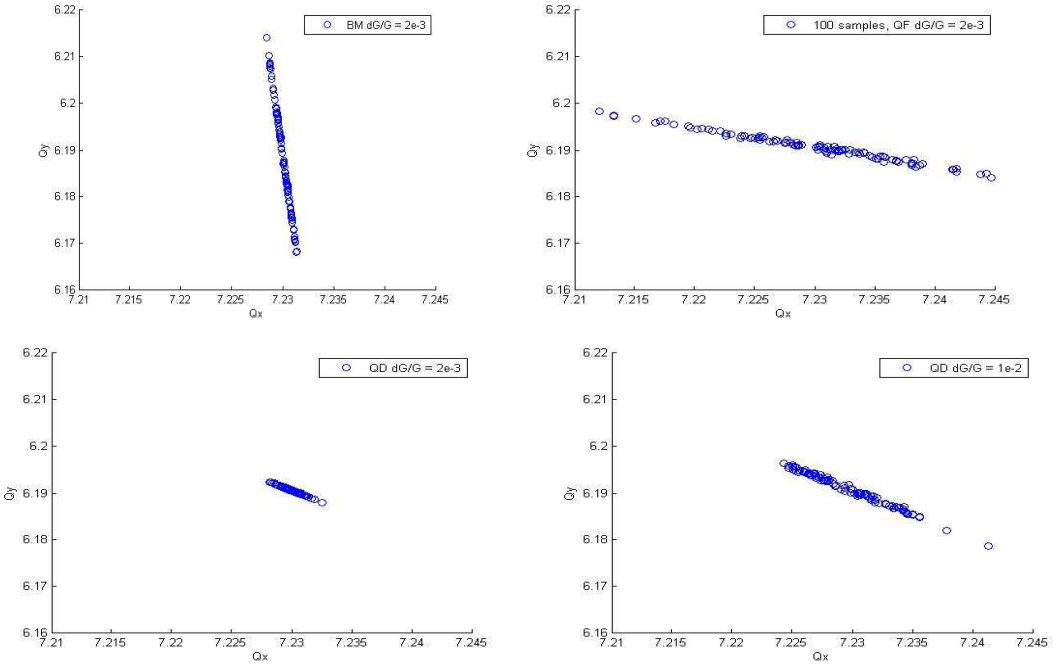


Figure 5: An example showing the effect of QD gradient error compared to those in QF and bending magnets. Tune shift due to: (top-left) dG/G= 2 $x10^{-3}$ in bending magnet, (top-right) dG/G= 2 $x10^{-3}$ in QF quadrupole, (bottom-left) dG/G= 2 $x10^{-3}$ in QD quadrupole, and (bottom-right) dG/G= 1 $x10^{-2}$ in QD quadrupole.

Figure 6 shows impact of sextupole gradient error on dynamic aperture. The tracking is done for 2000 turns, and chromaticities +5 in both planes.

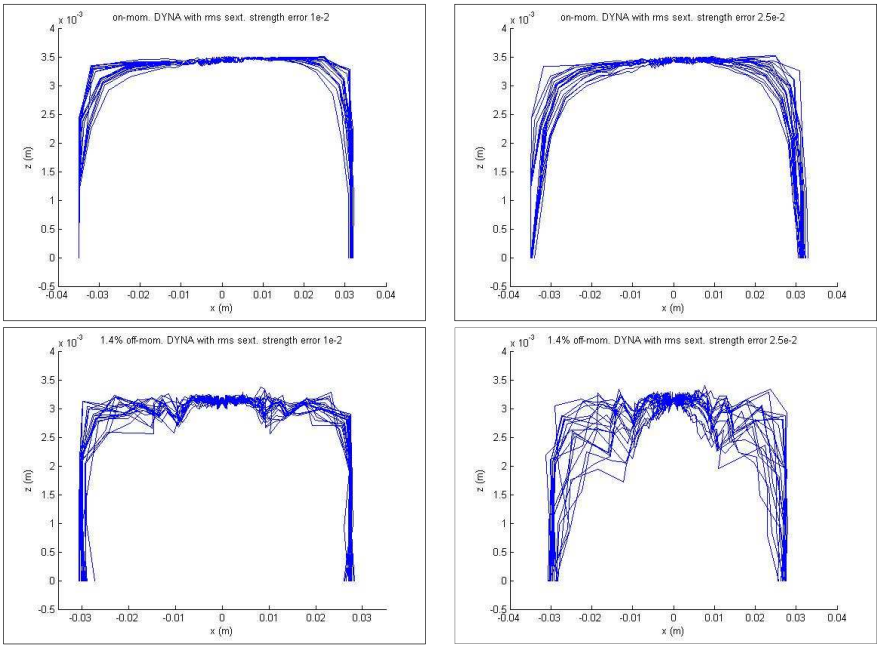


Figure 6: 20 samples of dynamic aperture, tracked for 2000 turns, in 4 cases: (top-left) on-momentum particle with dk/k = 1e-2, (top-right) on-momentum particle with dk/k = 2.5e-2, (bottom-left) 1.4% off-momentum particle with dk/k = 1e-2, and (bottom-right) 1.4% off-momentum particle with dk/k = 2.5e-2.

However, taking into account other sources of dynamic aperture destruction like the high order multipoles, ***the gradient error should be $\Delta(Gl)/Gl \leq 2\ x10^{-3}$ in bending magnet and QF quadrupole, while $\Delta(Gl)/Gl \leq 1\ x10^{-2}$ in QD quadrupole and sextupoles. The error distribution cutoff at $2\sigma$.***

## 5. The high order multipoles

The magnetic field errors represented by the high order multipoles modify the tunes shift with transverse oscillation amplitudes causing the working point to cross destructive resonances at lower oscillation amplitudes which reduces in turn the dynamic aperture size and, consequently, injection efficiency and beam lifetime. The main criterion used here in defining the lattice tolerance to high order multipoles is the dynamic aperture for chromaticities corrected to +5 in both planes. The multipole strength is calculated at x = ±20 mm in bending magnet and x = ±24 mm in quadrupoles and sextupoles.

The undesired high order multipoles are classified into *systematic multipoles* which are allowed by the magnet poles symmetry, and *random multipoles* which are created due to the different construction errors in the magnet. The systematic multipoles in the **2N**-pole magnet are **2N(2k + 1)**, where **N** = 1, 2, 3 for dipole, quadrupole, and sextupole respectively, and **k** = 1, 2, 3, …etc.
Concerning the random multipoles, the SESAME Quadrupoles and Sextupoles are assembled from individual poles. Hence, small displacement of an individual pole will cause random multipole components. The same is the case for powering the corrector coils, which are located around the sextupole coils. Although such components can be determined by FEM Programs like OPERA, an estimate can be done by using the perturbation theory from Halbach and the coefficients given by him. Following this theory, and using **N** for order of main pole (2 for quadrupole), **n** for order of corrected multipole, **ε** for current, radial or azimuthal distortion (dI/I, dr/r, dφ/φ), **m** = 1, 3, 5, 7 for quadrupole, and 1, 3, 5, 7, 9, 11 for sextupole, the disturbance is given by

$$\frac{B_n}{B_N} = c_{Nn} \sum \varepsilon_m \, e^{-i\left(\frac{nm}{N\pi}\right)} \qquad (1)$$

with the values of $\mathbf{c_{Nc}}$ coefficient listed in Table 2.

| $\mathbf{c_{Nn}}$ | | | | | | |
|---|---|---|---|---|---|---|
| N = 2 | | | | N = 3 | | |
| n | dI/I | dr/r | dφ/φ | dI/I | dr/r | dφ/φ |
| 1 | 0.199 | -0.425 | 0.075 | 0.098 | -0.314 | 0.051 |
| 2 | 0.25 | -0.516 | 0.214 | 0.156 | -0.495 | 0.171 |
| 3 | 0.157 | -0.288 | 0.288 | 0.167 | -0.515 | 0.303 |
| 4 | 0 | 0.068 | 0.231 | 0.133 | -0.39 | 0.39 |
| 5 | 0.021 | 0.108 | 0.108 | 0.071 | -0.173 | 0.397 |

Table 2: Coefficients for calculating higher multipole components given by Halbach.

For example a radial displacement of one pole (m=1) by 0.1 mm for a quadrupole with 35 mm pole radius will give the following decapole term at the pole radius $\frac{B_5}{B_2} = \frac{0.1}{35} * 0.108 * e^{-i\left(\frac{5}{4\pi}\right)}$
If the Multipoles are evaluated at a different radius ($r_m$) the new values are given as follows:

$$\frac{B_n}{B_N}(r_m) = \frac{B_n}{B_N}(r_p) * (\frac{r_m}{r_p})^{n-N} \quad (2)$$

The high order multipoles due to displacement of one pole of the focusing quadrupole, the defocusing sextupole, and due to exciting corrector coils of the defocusing sextupole, for example, are listed in Tables 3, 4, and 5 respectively.

| $B_n/B_2$ | | | | | | |
|---|---|---|---|---|---|---|
| | dr/r = .1/35; m = 1 | | dφ/φ .1/35; m = 1 | | dx/x .14/35; m = 1 | |
| n | normal | skew | normal | skew | normal | skew |
| 1 | -0.0013 | -0.0013 | 0.0002 | -0.0002 | -0.0011 | -0.0007 |
| 2 | -0.0015 | 0.0000 | 0.0000 | -0.0006 | -0.0011 | 0.0004 |
| 3 | -0.0004 | 0.0004 | -0.0004 | -0.0004 | 0.0000 | 0.0006 |
| 4 | 0.0000 | -0.0001 | -0.0003 | 0.0000 | 0.0002 | -0.0001 |
| 5 | -0.0001 | -0.0001 | -0.0001 | 0.0001 | 0.0000 | -0.0001 |

Table 3: Higher Multipoles for displacement of one pole (m =1) of the focusing quadrupole.

| $B_n/B_3$ | | | | | | |
|---|---|---|---|---|---|---|
| | dr/r = .1/35; m = 1 | | dφ/φ .1/35; m = 1 | | dx/x .14/35; m = 1 | |
| n | normal | skew | normal | skew | normal | skew |
| 1 | -0.0010 | -0.0017 | 0.0003 | -0.0002 | -0.0009 | -0.0011 |
| 2 | -0.0018 | -0.0010 | 0.0004 | -0.0006 | -0.0015 | -0.0003 |
| 3 | -0.0015 | 0.0000 | 0.0000 | -0.0009 | -0.0011 | 0.0006 |
| 4 | -0.0007 | 0.0004 | -0.0004 | -0.0007 | -0.0002 | 0.0007 |
| 5 | -0.0001 | 0.0002 | -0.0005 | -0.0003 | 0.0002 | 0.0003 |

Table 4: Higher Multipoles for displacement of one pole (m = 1) of the defocusing sextupole.

| $B_n/B_3$ (r= .0375) | | | | | | |
|---|---|---|---|---|---|---|
| | Horizontal correction | | Vertical correction | | Skew correction | |
| | dI/I = [1, 2, 1, -1, -2, -1] for m = [1, 3, 5, 7, 9, 11] | | dI/I = [1, -1, -1, 1] for m = [1, 5, 7, 11] | | dI/I = [1, 1] for m = [3, 9] | |
| n | normal | skew | normal | skew | normal | skew |
| 1 | 0.5880 | 0.0000 | 0.0000 | 0.3395 | 0.0000 | 0.0000 |
| 2 | 0.0000 | 0.0000 | 0.0000 | 0.0000 | 0.0000 | -0.3120 |
| 3 | 0.0000 | 0.0000 | 0.0000 | 0.0000 | 0.0000 | 0.0000 |
| 4 | 0.0000 | 0.0000 | 0.0000 | 0.0000 | 0.0000 | 0.2660 |
| 5 | 0.4260 | 0.0000 | 0.0000 | -0.2460 | 0.0000 | 0.0000 |

Table 5: Higher Multipoles for exciting the corrector coils of the defocusing sextupole.

The parameters of defocusing sextupole used are N*I = 3200 A.turns, and B = 0.32 T. Parameters of the correctors are corrector maximum kick = 0.5 mrad, corrector field = 0.023 T, corrector length = 0.18 m, N*I = 400 A.turn for horizontal corrector, and 700 A.tunrs for the vertical one.

The total transverse magnetic field expansion is given by [4]:

$$B_z + iB_x = \sum_{n=1}^{\infty}(b_n + ia_n)(x + iz)^{n-1} \quad (3)$$

where $B_z$, $B_x$ are the vertical and horizontal magnetic flux, $b_n$ and $a_n$ are the normal and skew multipole coefficients respectively. Assuming no considerable skew magnets in the storage ring yields $a_n$ = 0, with alignment errors are not taken into account. By expanding equation (3) and considering the terms related to the vertical magnetic flux $B_z$ we obtain:

$$B_z(x,z) = b_1 + b_2 x + b_3(x^2 - z^2) + b_4(x^3 - 3\,x\,z^2) + b_5(x^4 - 6\,x^2\,z^2 + z^4) + \ldots \qquad (4)$$

where $b_n(T/m^{n-1}) = \frac{1}{(n-1)!}\left(\frac{\partial^{n-1}B_z}{\partial x^{n-1}}\right)_{x=z=0}$ [5] is the gradient of the 2*n*-pole component for $n \geq 2$, while it is considered as the design orbit magnetic flux $B_0$ when $n = 1$. The strength of the 2*n*-pole component is $k_n(m^{-n}) = \frac{b_n}{B_0\rho_0} = \frac{1}{B_0\rho_0}\frac{1}{(n-1)!}\left(\frac{\partial^{n-1}B_z}{\partial x^{n-1}}\right)_{x=z=0}$ where $B_0\rho_0$ is the electron beam rigidity. The 2*n*-pole high order component is treated as a 2*n*-pole magnet extends over the main magnet in which it appears. The integrated strength of this 2*n*-pole magnet is given by $k_n L_m$ where $L_m$ is the magnetic length of the hosting main magnet. Any higher order multipole component is an error in magnetic flux $\Delta\boldsymbol{B}_z$ over the needed nominal one $\boldsymbol{B}_N$. The maximum relative error in the magnetic flux $\Delta\boldsymbol{B}_z$ / $\boldsymbol{B}_N$ that is tolerable by the lattice should be determined. By rewriting Eq. (4) in the form $B_z = B_1 + B_2 + B_3 + B_4 + \cdots + B_n$, the high order multipole errors in dipoles, quadrupoles and sextupoles are represented by $(\Delta B/B)_{2n-pole} = \frac{B_n}{B_1}, \frac{B_n}{B_2}, \frac{B_n}{B_3}$ respectively.

The high order multipole component is introduced to the lattice as a thin lens with integrated strength equivalent to that of the real one. In the bending magnet, it is divided into 3 equal parts inserted at the entrance, middle and exit of the bending magnet. In the quadrupole, the multipole component is inserted as one part in the middle of quadrupole, whereas in sextupole, the multipole component is inserted as one part near to the thin-lens modeled sextupole.

Concerning the convenient number of turns for particle tracking, Fig. 7 shows that 2000 and 5000 turns tracking give almost the same results. So, tracking the particle for 2000 turns is sufficient for the investigation, nevertheless it is tracked for 5000 turns for the final results.

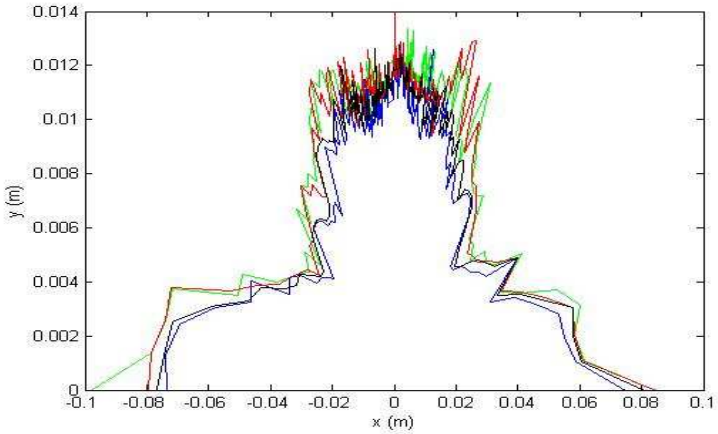


Figure 7: The dynamic aperture as a function of number of tracking turns: 5000 turns (blue), 2000 turns (black), 1000 turns (red), and 500 turns (green).

The 6-pole components is not taken into account here since it was investigated before and found to be not critical. The corresponding field error can be relaxed to $(\Delta B/B)_{6\text{-pole}} = 5 \times 10^{-3}$ without any problem on the dynamic aperture and can be easily compensated by the already low-strength sextupoles.

Finally, the strategy followed in this report is to define first the tolerance of each high order multipole component individually, which gives an idea also about the destruction effectiveness of each component. Then, to simulate the realistic case we combine all the multipole contents in all the magnets together using their defined tolerances. If the total effect becomes out of the lattice tolerance, the strengths of the components are reduced one by one starting with the most destructive components till we obtain a tolerable total effect.

### 5.1. High order multipoles in the dipoles (bending magnets):

Figure 8 shows impact of each dipole content, with different signs, from 8-pole up to 28-pole. The particles are tracked for 2000 turns with initial conditions spacing of x = 0.8mm, z = 0.2 mm.

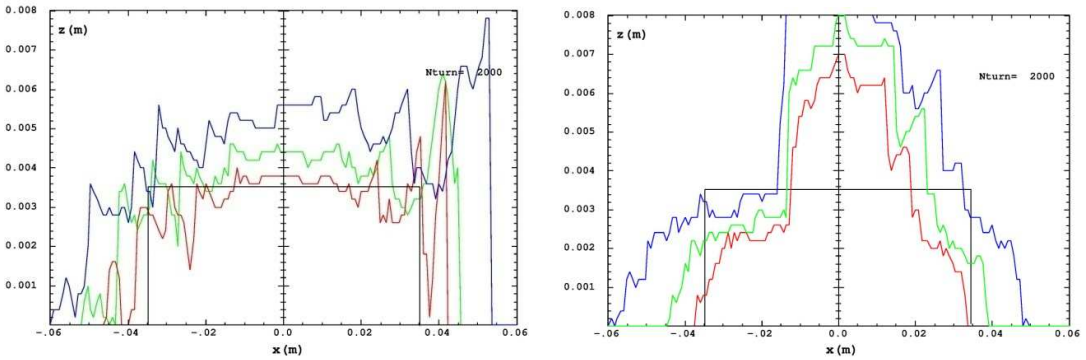


Figure 8.a: (Left) 8-pole error ΔB/B = 1e-3 (blue), 1.5e-3 (green), 2e-3 (red). (Right) the same values with negative sign.

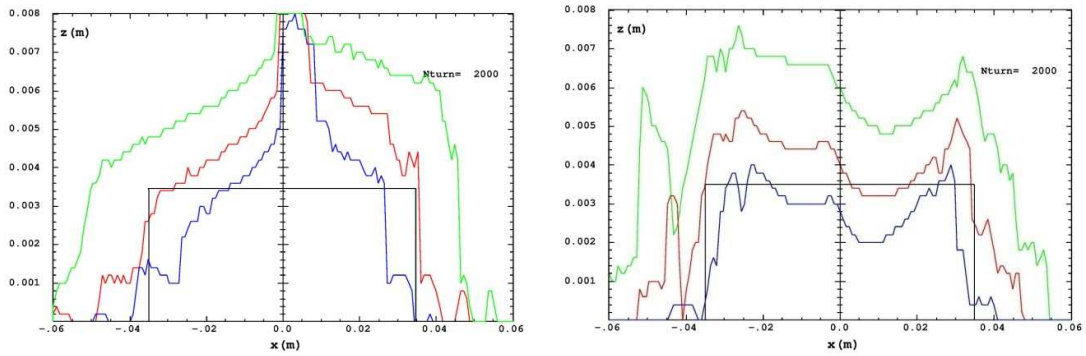


Figure 8.b: (Left) 10-pole error ΔB/B = 5e-4 (green), 1e-3 (red), 2e-3 (blue). (Right) the same values with negative sign.

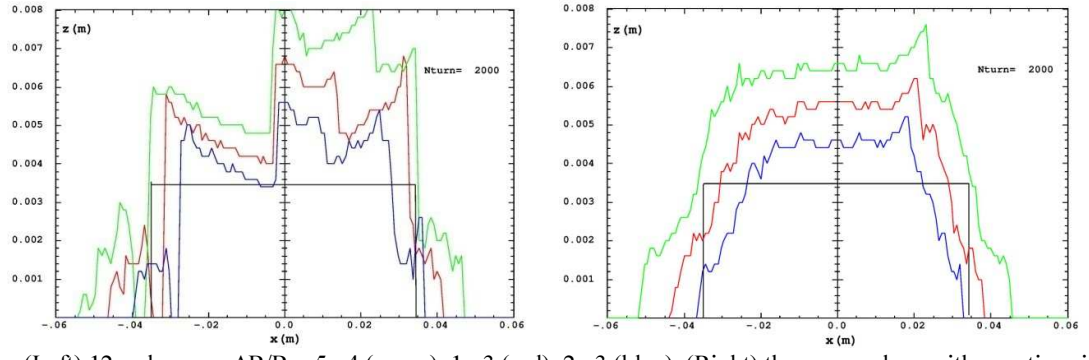


Figure 8.c: (Left) 12-pole error ΔB/B = 5e-4 (green), 1e-3 (red), 2e-3 (blue). (Right) the same values with negative sign.

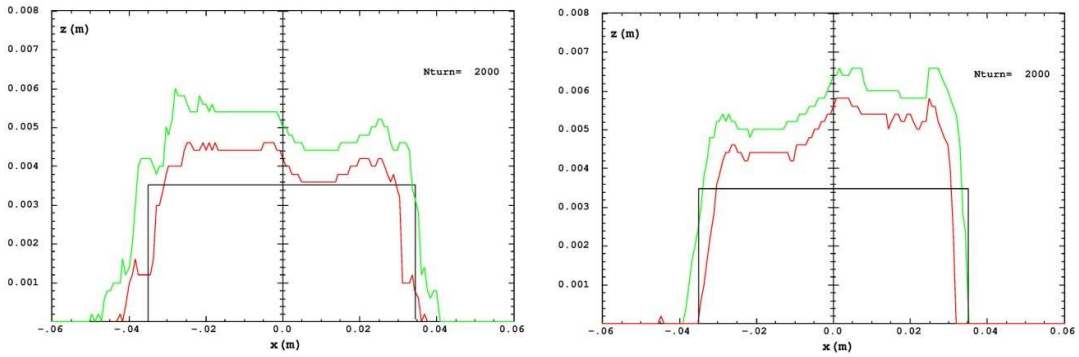


Figure 8.d: (Left) 14-pole error ΔB/B = 5e-4 (green), 1e-3 (red), 2e-3. (Right) the same values with negative sign.

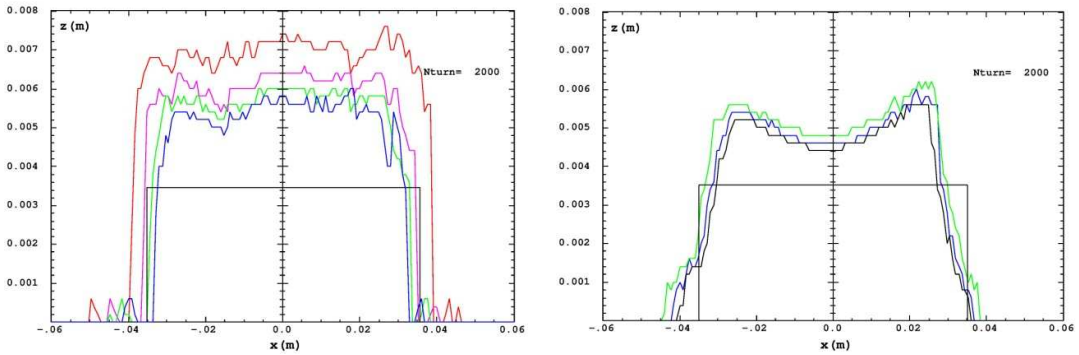


Figure 8.e: (Left) 16-pole error ΔB/B = 2e-4 (red), 4e-4 (pink), 6e-4 (green), 8e-4 (blue). (Right) the same values with negative sign.

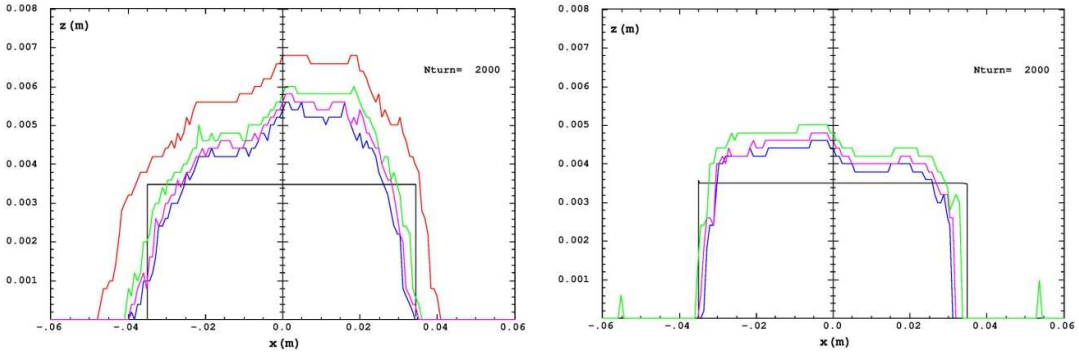


Figure 8.f: (Left) 18-pole error ΔB/B = 2e-4 (red), 6e-4 (green), 8e-4 (pink), 1e-3 (blue). (Right) the same values with negative sign.

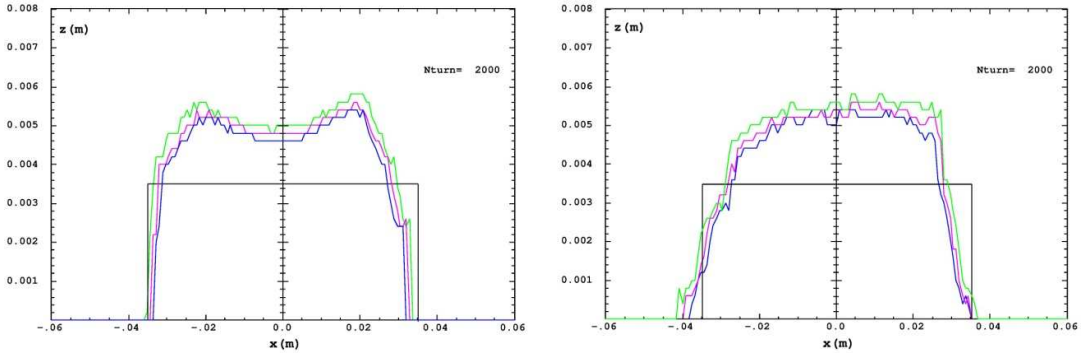


Figure 8.g: (Left) 20-pole error ΔB/B = 6e-4 (green), 8e-4 (pink), 1e-3 (blue). (Right) same values with negative sign.

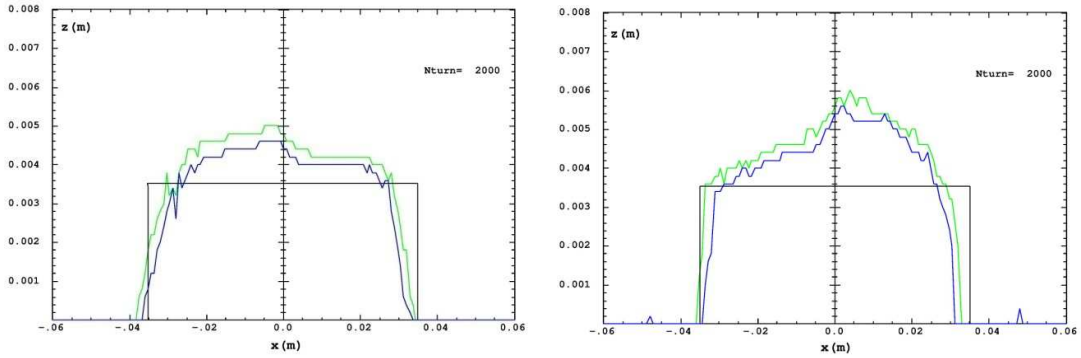


Figure 8.h: (Left) 22-pole error ΔB/B = 6e-4 (green), 1e-3 (blue). (Right) the same values with negative sign.

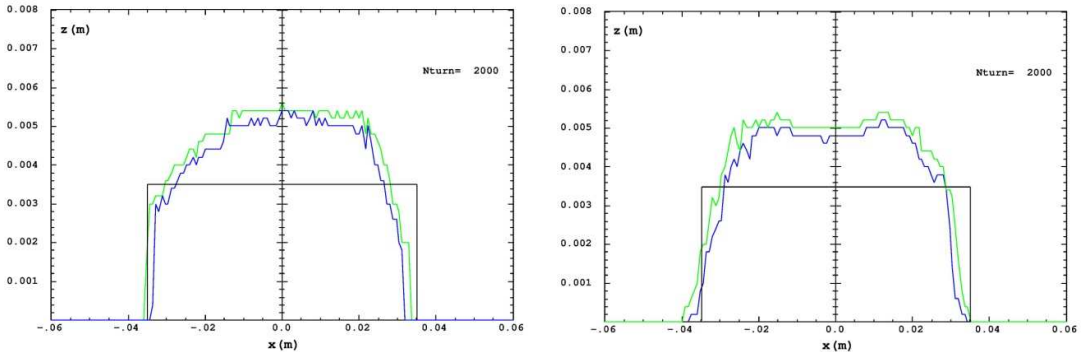


Figure 8.i: (Left) 24-pole error ΔB/B = 6e-4 (green), 1e-3 (blue). (Right) the same values with negative sign.

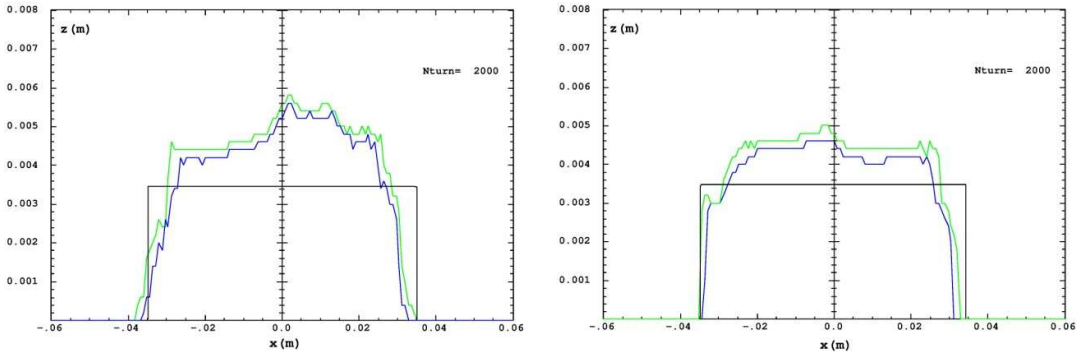


Figure 8.j: (Left) 26-pole error ΔB/B = 6e-4 (green), 1e-3 (blue). (Right) the same values with negative sign.

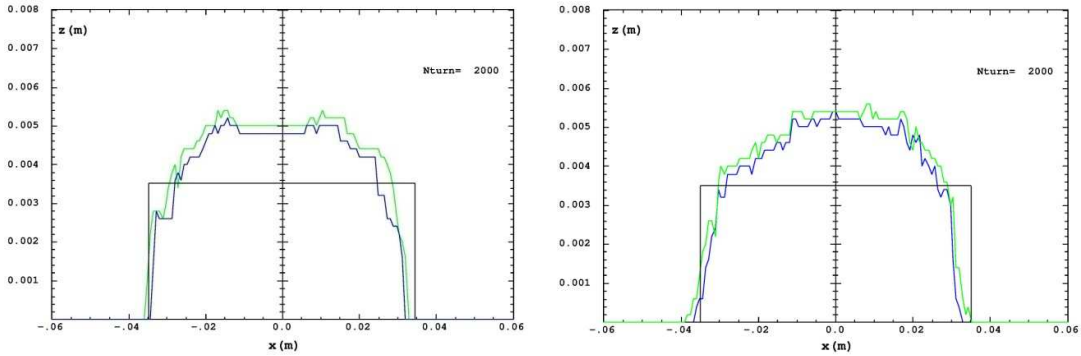


Figure 8.k: (Left) 28-pole error ΔB/B = 6e-4 (green), 1e-3 (blue). (Right) the same values with negative sign.

Figure 8: Effect of the different high order multipoles in bending magnet on the dynamic aperture. The particle is tracked for 2000 turns.

It can be seen that effect of the bending magnet contents is more critical in the vertical plane due to the high vertical beta function $\beta_z$ there which reaches 27 m in the middle of the dipole. Depending on the results of Fig. 7, the values of high order multipole tolerances are listed in Table 6.

| Multipole | 8 pole | 10 pole | 12 pole | 14 pole | 16 pole | 18 pole | 20 pole | 22 pole | 24 pole | 26 pole | 28 pole |
|---|---|---|---|---|---|---|---|---|---|---|---|
| Tolerance value | $\pm 1.5\times10^{-3}$ | $\pm 1\times10^{-3}$ | $\pm 1\times10^{-3}$ | $\pm 1\times10^{-3}$ | $\pm 6\times10^{-4}$ | $\pm 6\times10^{-4}$ | $\pm 6\times10^{-4}$ | $\pm 6\times10^{-4}$ | $\pm 6\times10^{-4}$ | $\pm 6\times10^{-4}$ | $\pm 1\times10^{-3}$ |

Table 6: Tolerances on high order multipoles in the bending magnet.

### 5.2. High order multipoles in the quadrupoles

In the quadrupole case, the 1st three systematic multipoles 12-pole, 20-pole, and 28-pole are considered, in addition to the random 8-pole, 10-pole, skew 6-pole, skew 8-pole, and skew 10-pole which are expected to be the main ones due to construction errors. Figures 9, 10 show impact of the systematic and random multipole components on the dynamic aperture.

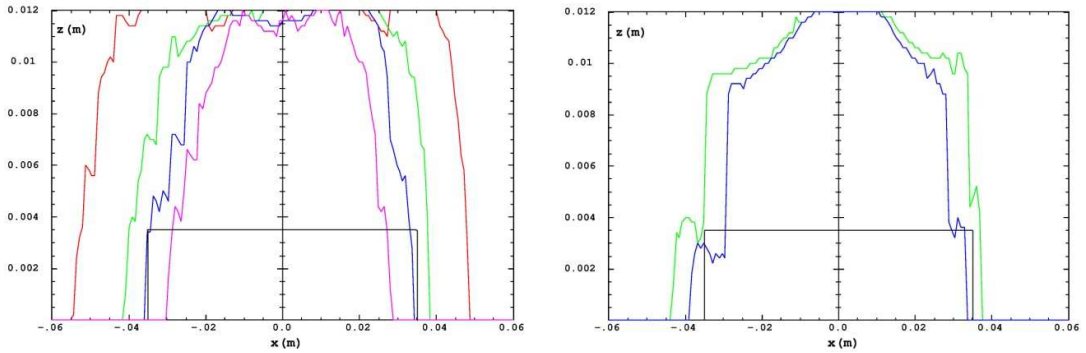


Figure 9.a: (Left) 12-pole error ΔB/B = 1e-3 (red), 3e-3 (green), 5e-3 (blue), 1e-2 (pink). (Right) ΔB/B = -3e-3 (green), -5e-3 (blue).

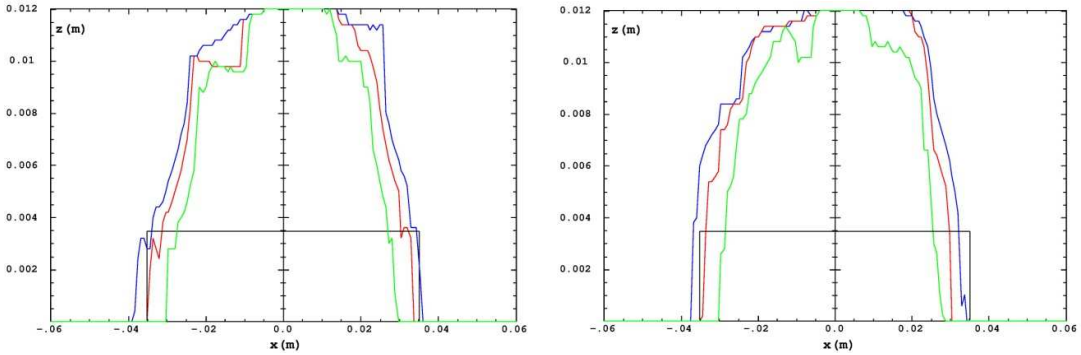


Figure 9.b: (Left) 20-pole error ΔB/B = 5e-4 (blue), 1e-3 (red), 3e-3 (green). (Right) the same values with negative sign.

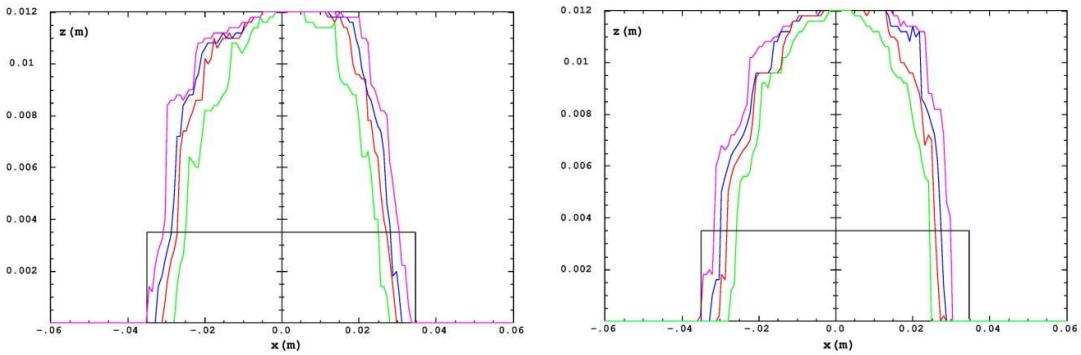


Figure 9.c: (Left) 28-pole error ΔB/B = 2e-4 (pink), 5e-4 (blue), 1e-3 (red), 3e-3 (green). (Right) the same values with negative sign.

Figure 9: Systematic high order multipoles in the quadrupole magnets.

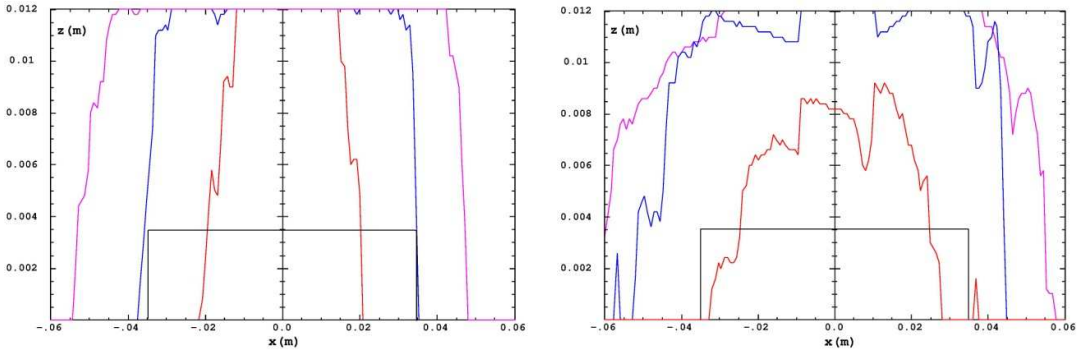


Figure 10.a: (Left) random 8-pole error ΔB/B = 5e-3 (pink), 1e-2 (blue), 3e-2 (red). (Right) same values with negative sign.

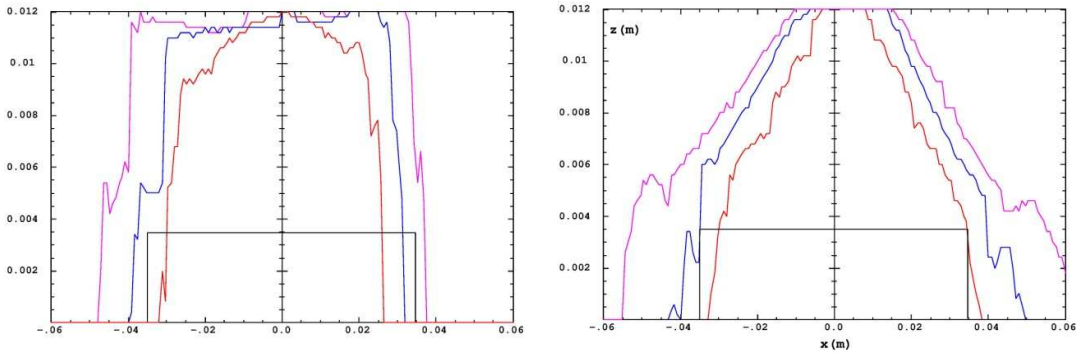


Figure 10.b: (Left) random 10-pole error ΔB/B = 5e-3 (pink), 1e-2 (blue), 2e-2 (red). (Right) the same values with negative sign.

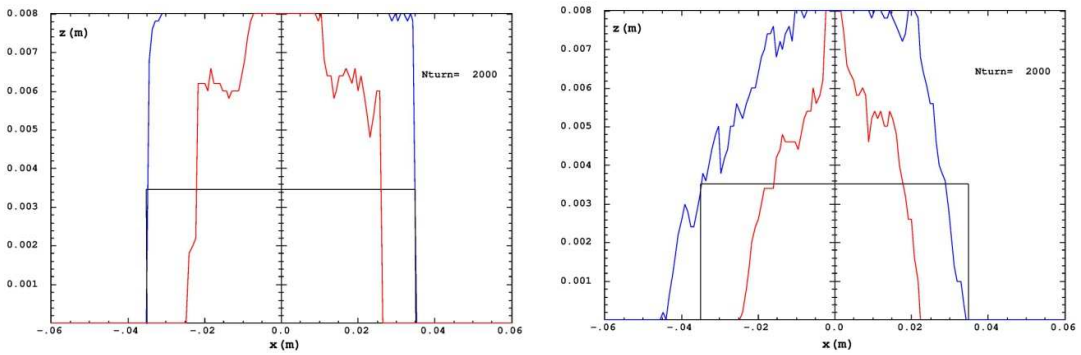


Figure 10.c: (Left) skew 6-pole error ΔB/B = 7e-2 (blue), 1e-1 (red). (Right) the same values with negative sign.

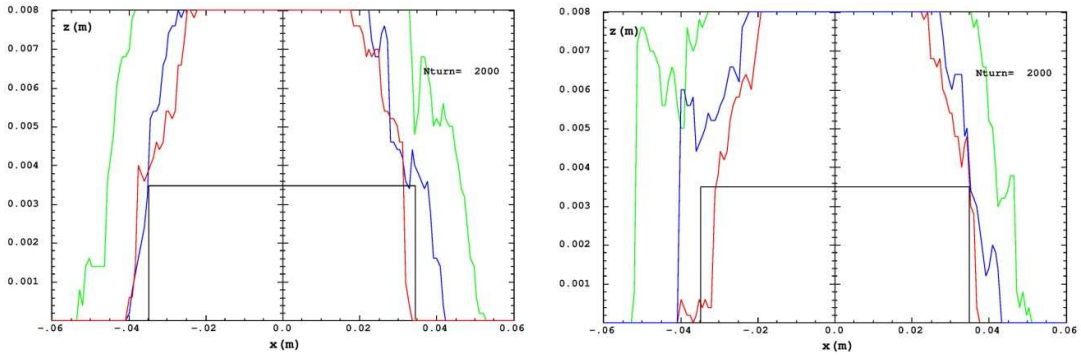


Figure 10.d: (Left) skew 8-pole error ΔB/B = 1e-2 (green), 1.5e-2 (blue), 2e-2 (red). (Right) same values with negative sign.

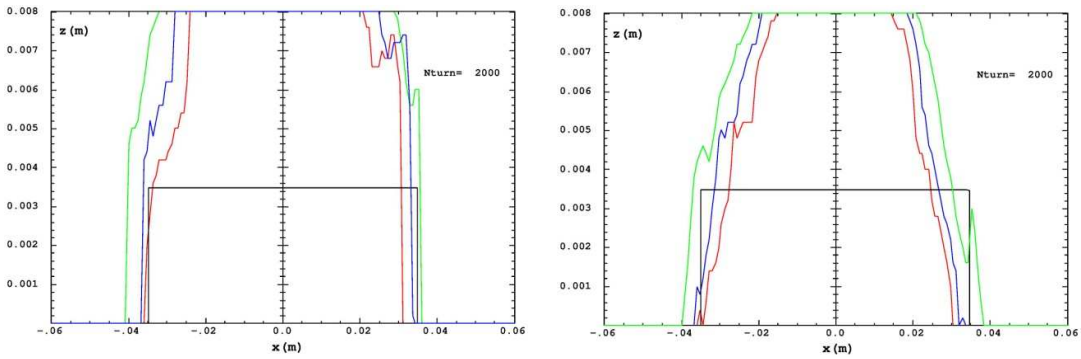


Figure 10.e: (Left) skew 10-pole error ΔB/B = 1e-2 (green), 1.5e-2 (blue), 2e-2 (red). (Right) the same values with negative sign.

Figure 10: Random high order multipoles in the quadrupole magnets.

Depending on the results in Figs. 9 and 10, the values of high order multipole tolerances are listed in Table 7.

| Multipole | Systematic 12-pole | Systematic 20-pole | Systematic 28- pole | Random 8-pole | Random 10-pole | Random Skew 6-pole | Random Skew 8-pole | Random Skew 10-pole |
|---|---|---|---|---|---|---|---|---|
| Tolerance value | $\pm 5 \times 10^{-3}$ | $\pm 1 \times 10^{-3}$ | $\pm 2 \times 10^{-4}$ | $\pm 1 \times 10^{-2}$ | $\pm 1 \times 10^{-2}$ | $\pm 7 \times 10^{-2}$ | $\pm 1.5 \times 10^{-2}$ | $\pm 1 \times 10^{-2}$ |

Table 7: Tolerances on high order multipoles in the quadrupole magnet.

### 5.3. High order multipoles in the sextupoles

In case of sextupoles, the 1st two systematic multipoles 18-pole and 30-pole are considered in addition to the random ones. The main random components created due to construction errors are normal and skew 8-pole and 10-pole components. Moreover normal and skew 10-pole component are created due to exciting the orbit correctors which are inserted in the sextupoles as rotating coils. Figures 11, 12 show impact of the systematic and random multipole components on the dynamic aperture. The skew 8-pole is not taken into account due to its negligible effect since its tolerance value is ΔB/B > 5e-1.

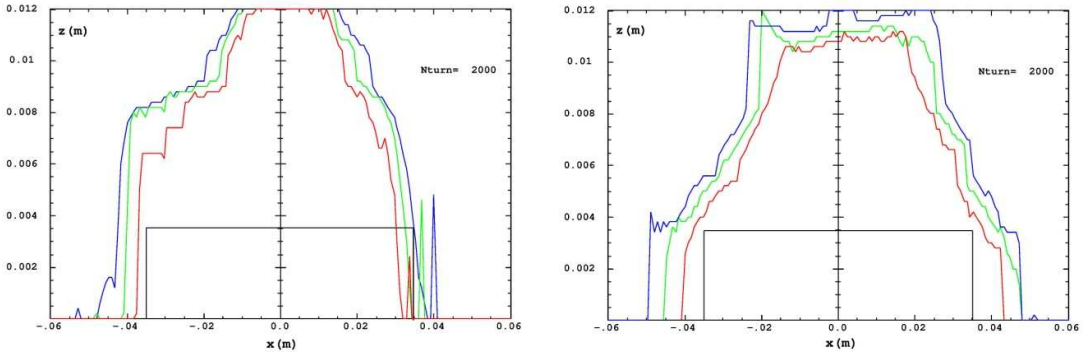


Figure 11.a: (Left) 18-pole error ΔB/B = 5e-3 (blue), 1e-2 (green), 2e-2 (red). (Right) the same values with negative sign.

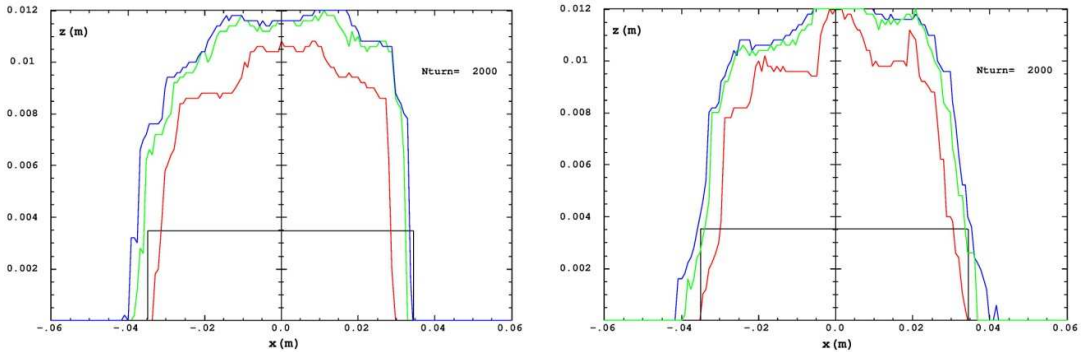


Figure 11.b: (Left) 30-pole error ΔB/B = 5e-4 (blue), 1e-3 (green), 5e-3 (red). (Right) the same values with negative sign.

Figure 11: Systematic high order multipoles in the sextupole magnets.

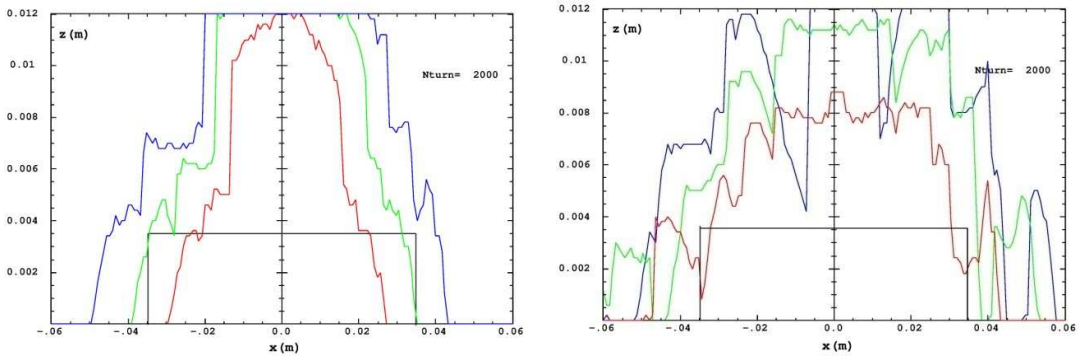


Figure 12.a: (Left) random 8-pole error ΔB/B = 2e-1 (blue), 3e-1 (green), 5e-1 (red). (Right) the same values with negative sign.

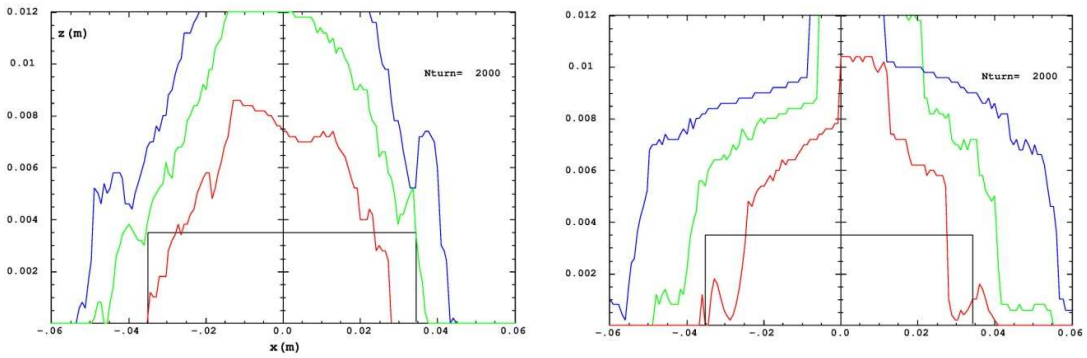


Figure 12.b: (Left) random 10-pole error ΔB/B = 1e-1 (blue), 2e-1 (green), 5e-1 (red). (Right) the same values with negative sign.

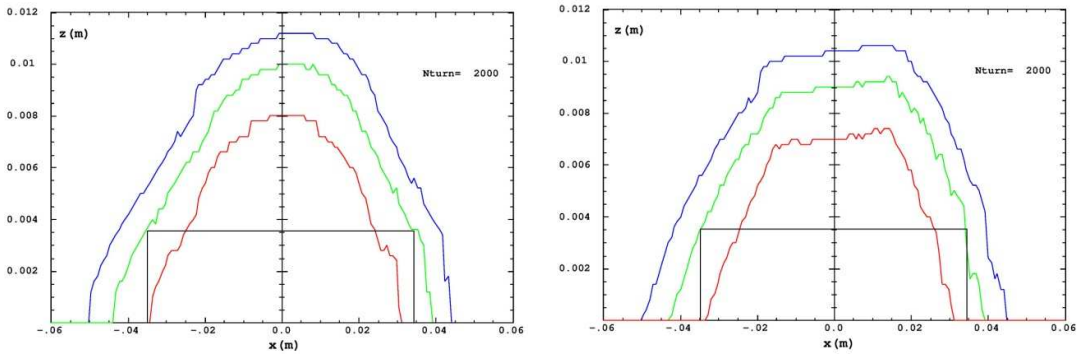


Figure 12.c: (Left) skew 10-pole error ΔB/B = 1e-1 (blue), 2e-1 (green), 5e-1 (red). (Right) the same values with negative sign.

Figure 12: Random high order multipoles in the sextupole magnets.

Depending on the results in Figs. 11 and 12, the values of high order multipole tolerances are listed in Table 8.

| Multipole | Systematic 18-pole | Systematic 30-pole | Random 8-pole | Random 10-pole | Random Skew 10-pole |
|---|---|---|---|---|---|
| Tolerance value | $\pm 2 \times 10^{-2}$ | $\pm 1 \times 10^{-3}$ | $\pm 3 \times 10^{-1}$ | $\pm 2 \times 10^{-1}$ | $\pm 2 \times 10^{-1}$ |

Table 8: Tolerances on high order multipoles in the sextupole magnet.

### 5.4. The dynamic aperture with all high order multipoles

However by including all the above high multipoles, in order to simulate the real case, the dynamic aperture has shrink to less than the physical acceptance required for the stored beam. By reducing values of some of the above multipole tolerances (mainly in dipoles and quadrupoles), keeping them reasonable, the dynamic aperture was enhanced and became acceptable from beam dynamics point of view. This is shown in Fig. 13, whereas the corresponding high order multipole tolerances are listed in Table 9.

Figures 14 and 15 show dynamic aperture and tune shift with amplitudes for two conservative cases in which all Table 4 high order multipoles have either positive sign or negative sign.

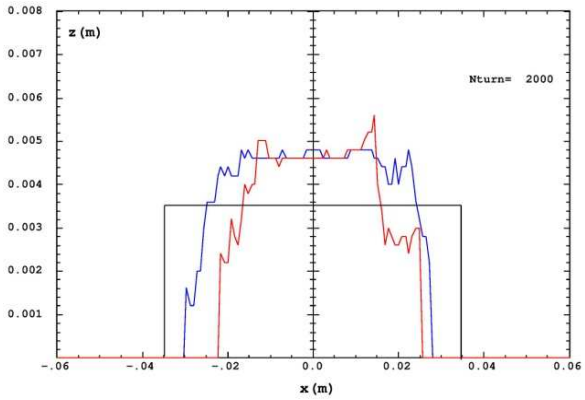


Figure 13: The dynamic aperture before (i.e. using the tolerances of Tables 1, 2, and 3) (red) and after (i.e. using the tolerances of Table 4) (blue) modifications on high order multipole tolerances.

| Final high order multipole tolerances in Bending Magnets | | | | | | | | | | | |
|---|---|---|---|---|---|---|---|---|---|---|---|
| Multipole | 8 pole | 10 pole | 12 pole | 14 pole | 16 pole | 18 pole | 20 pole | 22 pole | 24 pole | 26 pole | 28 pole |
| Tolerance value $B_n/B_0$ | $\pm 1\times10^{-3}$ | $\pm 1\times10^{-3}$ | $\pm 6\times10^{-4}$ | $\pm 1\times10^{-3}$ | $\pm 6\times10^{-4}$ | $\pm 6\times10^{-4}$ | $\pm 6\times10^{-4}$ | $\pm 6\times10^{-4}$ | $\pm 6\times10^{-4}$ | $\pm 6\times10^{-4}$ | $\pm 1\times10^{-3}$ |

| Final high order multipole tolerances in Quadrupole Magnets | | | | | | | | |
|---|---|---|---|---|---|---|---|---|
| Multipole | Systematic 12-pole | Systematic 20-pole | Systematic 28- pole | Random 8-pole | Random 10-pole | Random Skew 6-pole | Random Skew 8-pole | Random Skew 10-pole |
| Tolerance value $B_n/B_2$ | $\pm 6\times10^{-4}$ | $\pm 1\times10^{-3}$ | $\pm 2\times10^{-4}$ | $\pm 1\times10^{-3}$ | $\pm 1\times10^{-3}$ | $\pm 2\times10^{-3}$ | $\pm 2\times10^{-3}$ | $\pm 1\times10^{-2}$ |

| Final high order multipole tolerances in Sextupole Magnets | | | | | |
|---|---|---|---|---|---|
| Multipole | Systematic 18-pole | Systematic 30-pole | Random 8-pole | Random 10-pole | Random Skew 10-pole |
| Tolerance value $B_n/B_3$ | $\pm 2\times10^{-3}$ | $\pm 1\times10^{-3}$ | $\pm 1\times10^{-1}$ | $\pm 1\times10^{-1}$ | $\pm 1\times10^{-1}$ |

Table 9: The final tolerance values of high order multipoles in Bending Magnets, Quadrupoles, and Sextupoles.

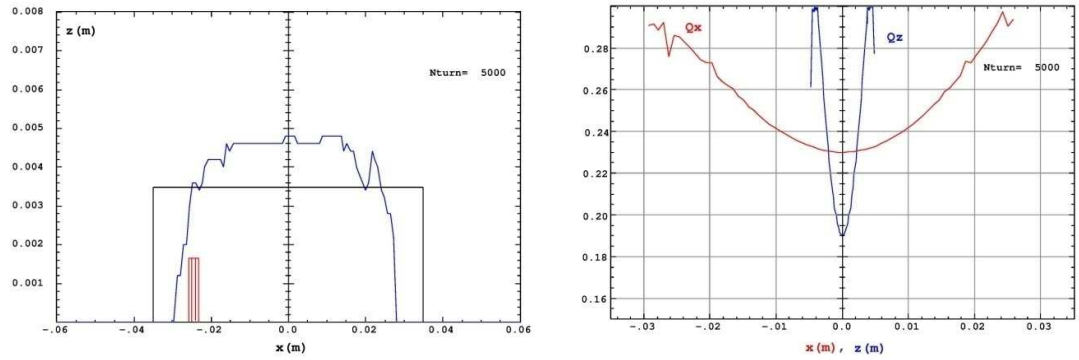


Figure 14: The dynamic aperture (left) and tune shift with amplitudes (right), with all multipoles of Table 9 having positive signs, compared to the aperture defined by the septum sheet which appears in red. The particle is tracked for 5000 turns.

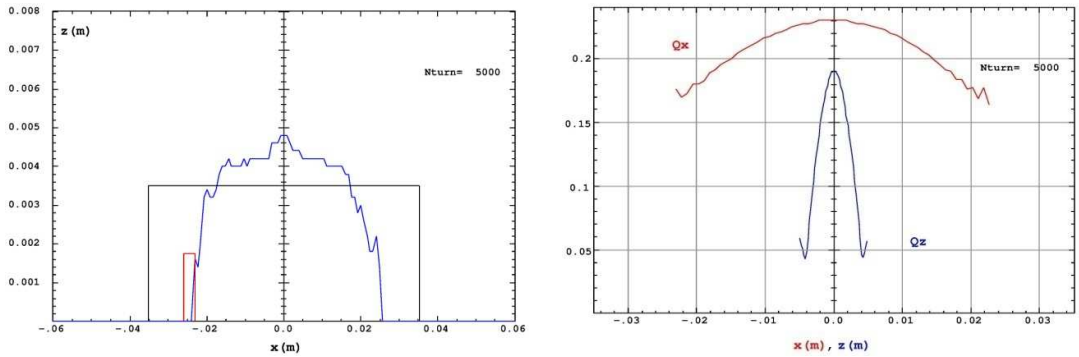


Figure 15: The dynamic aperture (left) and tune shift with amplitudes (right), with all multipoles of Table 9 having negative signs, compared to the aperture defined by the septum sheet which appears in red. The particle is tracked for 5000 turns.

### 5.4.1. More details using Frequency Map Analysis

In order to look deeper into the stability map over the dynamic aperture and to know in more details the reason behind the dynamic aperture destruction, the Frequency Map Analysis (FMA) technique [6, 7] is used. The case investigated using FMA is when all the multipole components of Table 9 have positive signs. Figures 16 and 17 show the stability structure of the absolute and chamber-limited dynamic apertures and the corresponding frequency maps for the on-momentum particle. The particle is tracked for 2048 turns using TRACY-2 code.

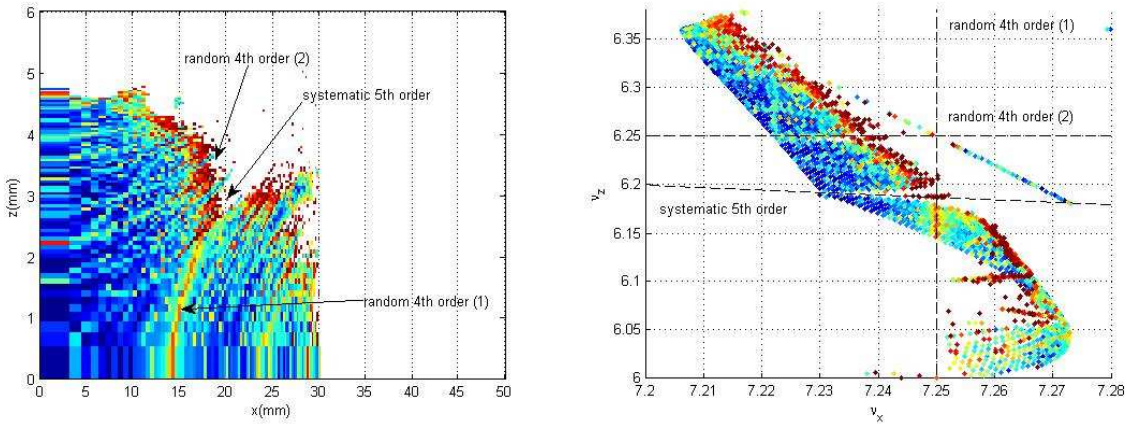


Figure 16: The absolute (i.e. vacuum chamber is not included) dynamic aperture with multipoles of Table 9 (left) and the corresponding frequency map (right). The particle is tracked for 2048 turns.

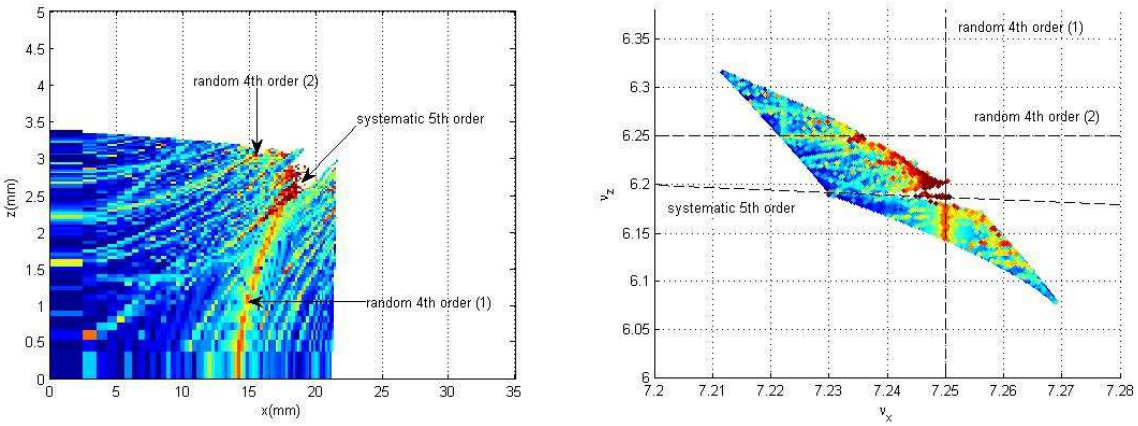


Figure 17: The chamber-limited (i.e. vacuum chamber is included in the tracking) dynamic aperture with multipoles of Table 9 (left) and the corresponding frequency map (right). The particle is tracked for 2048 turns.

Figure 16 shows a general shrink in the dynamic aperture caused by the particle instability that happens early at low transverse amplitudes due to the high order multipole effect. Moreover it shows clearly the effect of two main resonances; the random 4$^{th}$ order and the systematic 5$^{th}$ order ones listed in Table 10.

| Resonance | Resonance equation |
|---|---|
| Systematic 5$^{th}$ order | $Q_x + 4Qz = 32$ |
| Random 4$^{th}$ order (1) | $4Q_x = 29$ |
| Random 4$^{th}$ order (2) | $4Q_z = 25$ |

Table 10

The random 4$^{th}$ order resonance is excited by the octupole component which is created due to magnet construction errors, whereas the systematic 5$^{th}$ order one is a residual resonance around the working point however strengthened by the decapole component that is created by magnet construction errors.

Nevertheless the chamber-limited dynamic aperture in Fig. 17 shows that the physical acceptance defined by the vacuum chamber is not really harmed by the high order multipole effect, since the 5$^{th}$

order resonance effect doesn't propagate to low amplitudes whilst the nonlinearity created by the 4th order resonance seems not limiting for the dynamic aperture.
It is worth to mention that effect of 5th order resonance can be mitigated or even avoided by changing the fractional tunes [8]. However, a good construction for the magnets is the best way to mitigate the total high order multipole effect.

To have an idea about the multipole effect on off-momentum particles (consequently Touscheck beam lifetime), two cases are investigated using FMA, the ±1.5% off-momentum particles. Figure 18 shows the dynamic aperture of -1.5% off-momentum particle and the corresponding frequency map, whereas the corresponding resonances are listed in Table 11.

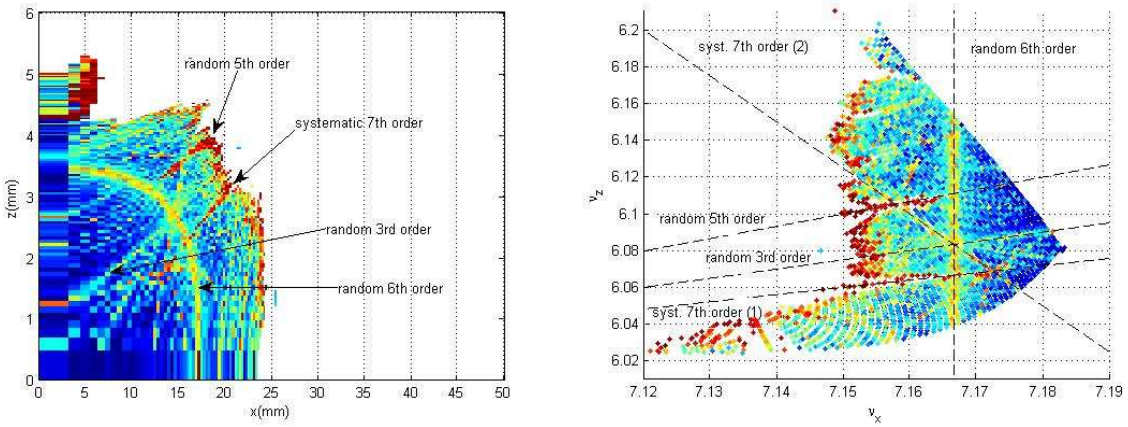


Figure 18: The absolute dynamic aperture for the -1.5% off-momentum particle with multipoles of Table 9 (left) and the corresponding frequency map (right). The particle is tracked for 2048 turns.

| Resonance | Resonance equation |
|---|---|
| Random 3rd order | $-Q_x + 2Q_z = 5$ |
| Random 5th order | $-2Q_x + 3Q_z = 4$ |
| Random 6th order | $6Q_x = 43$ |
| Systematic 7th order (1) | $-2Q_x + 5Q_z = 16$ |
| Systematic 7th order (2) | $5Q_x + 2Q_z = 48$ |

Table 11

Since the -1.5% off-momentum particle is shifted in tunes, it faces other types of resonances. Nevertheless, the destructive effect of the shown resonances decreases with lower transverse amplitudes which makes them less harmful for the stored beam. A similar case is seen in Fig. 19 for the 1.5% off-momentum particle.

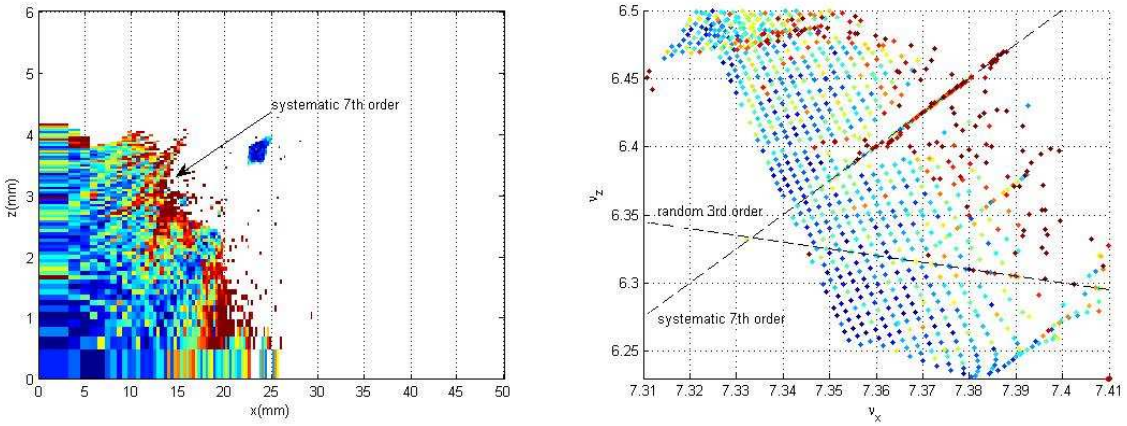


Figure 19: The absolute dynamic aperture for the 1.5% off-momentum particle with multipoles of Table 9 (left) and the corresponding frequency map (right). The particle is tracked for 2048 turns.

The above off-momentum calculations show also that the high order multipole errors of Table 9 are tolerable, however reducing them as much as possible is still preferred for a better machine performance.

**References**

[1] BETA, J. Payet. CEA/DSM/ Irfu/ SACM, ftp:// ftp.cea.fr/incoming/y2k01/beta/.
[2] A. Terebilo, SLAC-PUB-8732.
[3] J. Bengtsson, E.Forest and H. Nishimura, 'Tracy User Manual', unpublished (ALS, Berkeley).

[4] J. Rossbach, P. Schmuser, "*Basic Course on Accelerator Optics*", CERN Acc. Sch., Finland, September 1992, CERN 94-01.

[5] L. Farvacque, T.F. Günzel, J.L. Laclare, A. Ropert, "*BETA USERS' GUIDE*", Grenoble, third edition July 2001.

[6] J. Laskar, Icarus 88, 266-291 (1990).

[7] H. S. Dumas, J. Laskar, Phys. Rev. Lett. 70, 2975-2979 (1993).

[8] M. Attal, "Influence of the Vacuum Chamber Limitation on Dynamic Aperture Calculations", Proceedings of IPAC 13, Shanghai, China.